Zinc Dialkyl Dithiophosphate Antiwear Tribofilm and its Effect on the Topography Evolution of Surfaces: A Numerical and Experimental Study

Ali Ghanbarzadeh[1], Elio Piras[1,2], Ileana Nedelcu[2], Victor Brizmer[2], Mark C. T. Wilson[1], Ardian Morina[1], Duncan Dowson[1], Anne Neville[1]

[1] Institute of Functional Surfaces, School of Mechanical Engineering, University of Leeds, Leeds, UK

[2] SKF Engineering and Research Centre, the Netherlands

Corresponding authors:

E-mail address: *a.ghanbarzadeh@leeds.ac.uk (Ali Ghanbarzadeh)

*mnep@leeds.ac.uk (Elio Piras)

Abstract

A modelling framework has recently been developed which considers tribochemistry in deterministic contact mechanics simulations in boundary lubrication. One of the capabilities of the model is predicting the evolution of surface roughness with respect to the effect of tribochemistry. The surface roughness affects the behaviour of tribologically loaded contacts and is therefore of great importance for designers of machine elements in order to predict various surface damage modes (e.g. micropitting or scuffing) and to dessign more efficient tribosystems. The contact model considers plastic deformation of the surfaces and employs a modified localized version of Archard's wear equation at the asperity scale that accounts for the thickness of the tribofilm. The evolution of surface topography was calculated based on the model for a rolling/sliding contact and the predictions were validated against experimental results. The experiments were carried out using a Micropitting Rig (MPR) and the topography measurements were conducted using White Light Interferometry. Numerically, it is shown that growth of the ZDDP tribofilm on the contacting asperities affects the topography evolution of the surfaces. Scanning Electron Microscopy (SEM) and X-ray Photoelectron Spectroscopy (XPS) have been employed to confirm experimentally the presence of the tribofilm and its chemistry. The effects of the contact load and surface hardnesses on the evolution of surface topography have also been examined in the present work.

Key words: Surface Roughness, Boundary Lubrication, Tribochemistry, Wear, ZDDP

1. Introduction

Running-in is an important term used in the field of tribology. Due to the complexity and diversity of the phenomena occurring in this period various definitions of the term can be found in the literature (1). As described by Blau (2), running-in is a combination of processes that occur prior to the steady-state when two surfaces are brought together under load and with relative motion, and this period is characterized by changes in friction, wear and physical and chemical properties of surfaces. During the running-in period, surface micro topography is subjected to various changes. In boundary and mixed lubrication conditions, the height of the asperities of rough surfaces normally decrease (3-6). However, in the case of very smooth surfaces, an increase in the roughness value is observed (7, 8). During the process of change in the roughness of the surfaces, load carrying capacity is increased due to the gradual development of asperity-level conformity. The increase in the conformity of the surfaces is significant as peaks and valleys of the surfaces correspond to each other, and the overall performance of the system is improved (9-11).

Predicting changes in the topography of contacting bodies is important for designers to be able to predict the mechanical and chemical behaviour of surfaces in loaded tribological systems. The roughness of operating surfaces influences the efficiency of mechanical parts. In the design of machine elements and selection of materials, the film thickness parameter, known as the λ ratio, which is a representation of the severity of the contact, is important (12). Its value is inversely proportional to the composite roughness of the two surfaces in contact. It is also widely reported that fatigue life of bearing components is dependent on their functional surfaces' characteristics, such as roughness. Optimization of the surface roughness can help in increasing the lifetime of bearings based on their applications (13, 14). Surface roughness can enhance stress concentrations that can lead to surface-initiated rolling contact fatigue (15). Therefore, it is important to be able to predict the surface topography changes in a tribologically-loaded system.

The changes in topography can be either due to plastic deformation of the surface asperities or due to removal, loss or damage to the material, which is known as wear. Evaluating wear in boundary lubrication has been the subject of many studies. There are almost 300 equations for wear/friction in the literature which are for different conditions and material pairs but none of them can fully represent the physics of the problem and offer a universal prediction (16, 17). Some examples of these models are the Suh delamination theory of wear (18), the Rabinowicz model for abrasive wear (19) and the Archard wear equation (20, 21). Wear occurs by different interfacial mechanisms and all these mechanisms can contribute to changes in the topography. It has been widely reported that third body abrasive particles play an important role in changes in the topography of surfaces. There are several parameters that govern the wear behaviour in this situation such as wear debris particle size or shape, configuration of the contact and contact severity etc. (22-24). It was reported by Godet (25) that a comprehensive mechanical view of wear should consider the third body abrasive particles and their effect on wear and topography changes. A study of abrasive wear under three-body conditions was carried out by Rabinowicz et al (26). They proposed a simple mathematical model for third body abrasive wear rate and showed that the wear rate in this situation is about ten times less than two-body abrasive wear. It was reported by Williams et al. (27) that lubricant is used to drag the wear debris inside the interface and the abrasive wear action then depends on the particle size, its shape and the hardness of the materials. They reported that a critical ratio of particle size and film thickness can define the mode of surface damage. Despite the importance of a three-body abrasive wear mechanism there is no comprehensive mechanistic model to describe such a complicated mechanism. In the mild wear regime in lubricated contacts the effect of third body abrasive is often assumed to be insignificant.

Most of the work in the literature is based on using the well-known Archard wear equation to evaluate wear in both dry and lubricated contacts. Olofsson (28-30) used Archard's wear equation to evaluate wear in bearing applications and observed the same behaviour between model and experiments. Flodin (31) showed that Archard's wear equation is good enough to predict wear in spur helical gears application. Andersson et al (32) tested and reviewed different wear models and reported that Archard's wear model can predict wear of lubricated and unlubricated contacts and is able to predict the surface topography both in macro and micro-scales. They tested their generalized Archard's wear model for random rough surface contact (33). The Archard wear equation was widely used in numerical studies in order to predict the wear and topography at different scales (34-47).

Hegadekatte et al. (39) developed a multi-time-scale model for wear prediction. They used commercial codes to determine the contact pressure and deformations and then used Archard's wear equation to calculate wear. Andersson et al. (47) have employed the Archard wear equation to predict wear in a reciprocating ball-on-disc experiment. They used a wear model and implemented Fast Fourier Transforms (FFT) based contact mechanics simulations to calculate contact pressure and deformations. However, in all these implementations of Archard's wear equation in numerical models, which resulted in reasonably good agreement with experimental results, the effect of lubrication and lubricant properties was neglected. Recently, there have been some attempts to consider the lubrication effects in boundary lubrication modelling that could affect modifications to Archard's wear equation.

Bosman & Schipper (48) proposed a numerical model for mild wear prediction in boundary lubricated systems. They assumed that the main mechanisms that protect the boundary lubricated system are the chemically-reacted layers and when these layers are worn off, the system will restore the balance and the substrate will react with the oil to re-establish the tribofilm. They also proposed a transition from mild wear to more severe wear by making a complete wear map. In another recent work by Andersson et al. (49), contact mechanics of rough surfaces was used to develop a chemo-mechanical model for boundary lubrication. They used an Arrhenius-type thermodynamic equation to develop a mathematical model for formation of the tribofilm on the contacting asperities. They have also employed the mechanical properties of the antiwear tribofilm and used Archard's wear equation to predict wear of the surfaces. The coefficient of wear was assumed to be the same for the areas where the tribofilm is formed with the areas without the tribofilm.

Recent work by Morales Espejel et al. (50) used a mixed lubrication model to predict the surface roughness evolution of contacting bodies by using a local form of Archard's wear equation, and the model results show good agreement with experimental data. They used a spatially and time-dependent coefficient of wear that accounts for lubricated and unlubricated parts of the contact. The same modelling framework was used in other works of those authors to predict wear and micropitting (51).

A range of experimental work has investigated changes in surface roughness during tribological contacts. Karpinska (7) studied the evolution of surface roughness over time for both base oil and base oil with ZDDP. She also studied the wear of surfaces at different instants during running-in. It was suggested that a ZDDP tribofilm significantly affects the topographical changes of surfaces during running-in. Blau et al. (1) stated that friction and wear in running-in are time-dependent and related to the nature of energy dissipation in the contacts; they are governed by a combination of different mechanical and chemical processes. They showed that roughness evolution of contacting surfaces might have different patterns for both surfaces, depending on several parameters.

Despite the importance and the attempts in the literature to monitor and predict the roughness evolution of surfaces, there is no reported work that addresses the effect of tribochemistry. However, a modelling framework has recently been developed by the authors (52),(53) that is capable of predicting changes in surface topography under boundary lubrication conditions, taking into account the simultaneous dynamics of an anti-wear tribofilm. The present paper therefore seeks to test and exploit this model to explore the effect of a ZDDP tribofilm on the evolution of surface topography. The topography evolution of both contacting surfaces is predicted, taking into account not only the effects of plastic deformation and mild wear but also the coupled development and influence of a ZDDP antiwear tribofilm.

Experimental results from a Micropitting Rig (identical to the one used in Ref (50)) are used to validate the model in terms of general prediction of topography changes and growth of the ZDDP tribofilm on the contacting asperities. The numerical model is described briefly in Section 2, while the experimental set-up that the numerical model is adapted to is explained in Section 3. The numerical results based on the model are then reported and discussed in Section 4, where special attention is given to the different parameters in the model that affect the surface topography evolution. The importance of the growth of ZDDP tribofilm in changing the topography of surfaces in the model is shown in that section. The experimental results from the MPR and surface roughness measurements are reported in Section 5, where the thickness of the tribofilm and the evolution of surface roughness are compared with the numerical results of Section 4. Using the validated model, the effects of two important physical parameters – the hardness and the load – are studied numerically in Sections 6 and 7.

2. Numerical model

The numerical model used in this work is the one reported by the authors in Ref (52). The model is adaptable to tribosystems with different configurations which makes it possible to investigate different problems. The model consists of three important parts:

(i) A contact mechanics code for rough surfaces assuming an elastic-perfectly plastic material response;
(ii) A semi-analytical tribofilm growth model which includes both tribofilm formation and partial removal; and
(iii) A modified Archard's wear equation which accounts for the local thickness of the ZDDP tribofilm.

A brief description of the model is given below; further details on parts (i) and (ii) can be found in Ref (52) and an expanded discussion on part (iii) and the wear model validation is reported in (53). The whole numerical model algorithm is shown schematically in Figure 1.

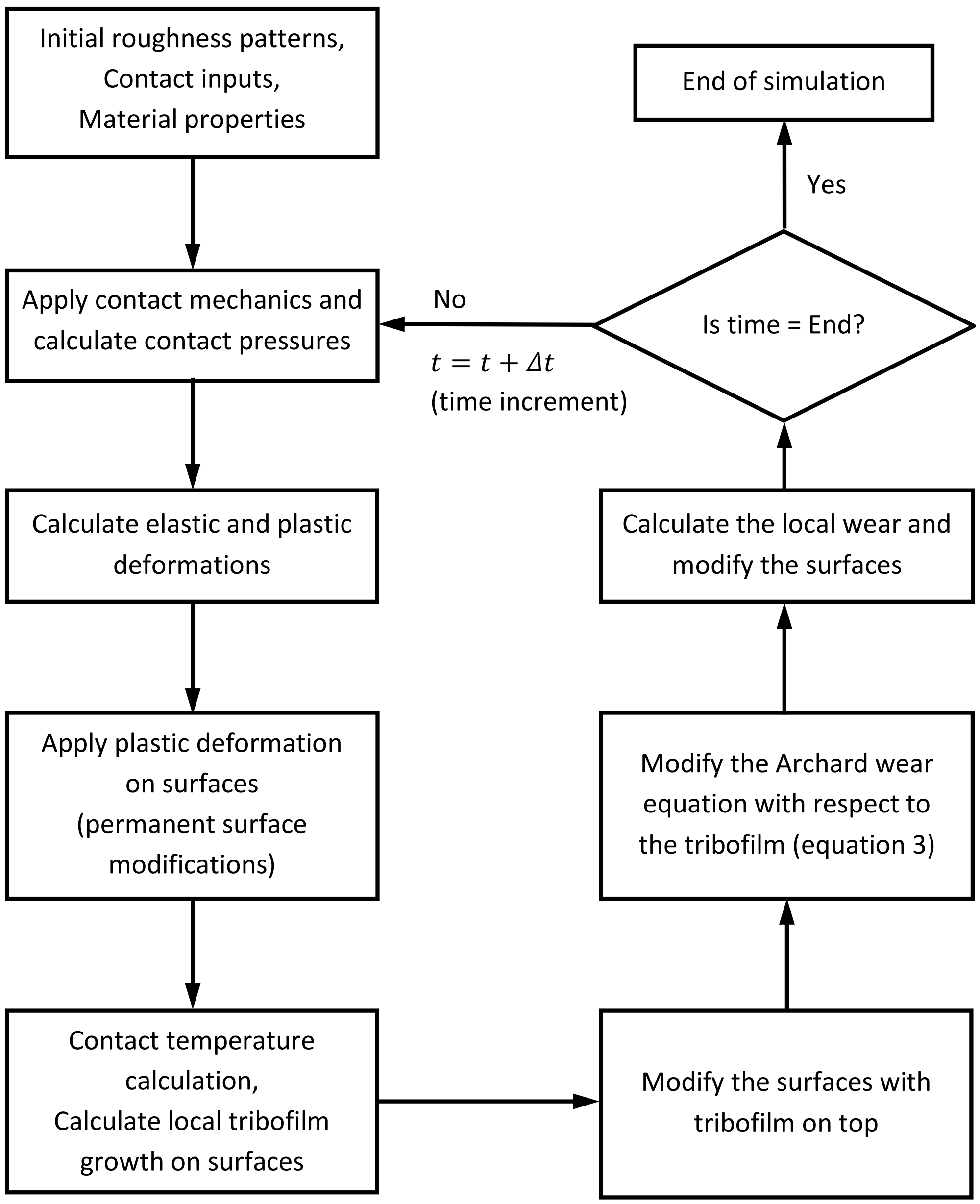

Figure 1. Flow chart for the numerical procedure.

Digitized surfaces are important inputs for the deterministic contact mechanics simulations. Surfaces are generated in this work based on the model developed by Tonder (54) which is based on the digital filtering of a Gaussian input sequence of numbers. This method generates surfaces with desired roughness and asperity lateral size. Using artificial surface topographies instead of actual surface scans does have some drawbacks, but also several advantages. For practical reasons, it is good to use the measured surface topography to study different cases for bearings, gears and other machine element parts. In addition, some important real characteristics of the engineering surface might be missed if using artificial generated surfaces. However, artificial surfaces can be used for scientific studies in different lubrication regimes, and they are particularly good for performing parametric studies independently of specific experimental datasets. It is possible to see the effect of different topographic properties on the tribofilm formation, plastic deformation, wear and topography evolution. The method is simple to manipulate and, since this work seeks to evaluate the performance of the model as a general tool for exploring topography evolution, is appropriate.

The contact mechanics model is based on the complementary potential energy concept using the model of Tian et al. (55). An elastic-perfectly plastic approach is then employed with the hardness of the material to be the criterion for the plastic flow. This assumption neglects the work hardening behaviour of the asperities as they deform. This method gives realistic contact pressure estimation but the deformations due to the pressure can be different from real values as the influence coefficients of an elastic material are used, neglecting the non-linear behaviour of the yielding subsurface material. Despite its shortcomings, this method has been widely used in the literature for modelling pressures and surface deformations in the elastic-plastic contacts. The model is based on the contact model by Sahlin et al (56). The surfaces move relative to each other and the slide-to-roll ratio determines the speed of the movement of surfaces. Therefore an asperity of one surface can contact with a number of asperities on its way. The movement of surfaces is periodic and is carried out by shifting the elements of matrices containing the values for the asperity heights.

The thermal model used to calculate the flash temperature is based on the Blok theory (57). It is obtained from calculation of the frictional heating. It should be noted that only the maximum temperature is important in this work and using Blok’s theory seems reasonable. The formulation used in this work is based on the equations reported in Kennedy and Tian (58, 59).

A tribochemical model was developed in the previous work of the authors that can capture the growth of the tribofilm on the asperity level. The tribofilm growth is taken to be a combination of the formation and partial removal at the same time (52). The formation of the tribofilm is assumed to be due to tribochemical reactions and follows the reaction kinetics based on the non-equilibrium thermodynamics of interfaces. The formation model is combined with a phenomenological term that accounts for the simultaneous partial removal of the tribofilm, giving the net development of the tribofilm thickness as a function of time:

$$h(t) = h_{max}\left(1 - e^{\left(-\frac{k_1 T}{h'} . x_{tribo} . t\right)}\right) - C_3(1 - e^{-C_4 t}) \qquad (1)$$

where k_1 and h' are the Boltzmann and the Planck constants respectively, T is the flash temperature and C_3 and C_4 are constants accounting for the continuous partial removal of the tribofilm. Hence the tribofilm is modelled as a dynamic system such that even when an equilibrium thickness is achieved, formation and partial removal continue but balance each other to maintain that thickness. Note that t in equation (1) refers to a local time for each point in the domain, and starts increasing at a given point once an asperity contact occurs there. The term x_{tribo} captures the effect of rubbing in inducing the tribochemical reactions. As reported recently (60), mechanical activation plays an important role in the growth behaviour of the tribofilm on a single asperity. Gosvami et al. (60) showed that the rate of tribochemical reaction is highly dependent on the pressure applied on a single asperity. This is in line with the model presented above, where the role of mechanical activation is represented by the term x_{tribo}. A detailed discussion can be found in the previous work (52).

At this point it is important to distinguish between the wear of the tribofilm, which is captured by the ‘partial removal’ term in Equation (1), and the wear of the substrate itself. Henceforth in this paper the term ‘wear’ will be used to refer to the (mild) wear of the substrate underneath the tribofilm – i.e. the wear of the substrate in the presence (and, initially, absence) of the tribofilm. Studies of ZDDP tribofilms on steel show that the tribofilm contains substrate atoms at a concentration that decreases towards the top of the tribofilm. Hence material from the substrate is consumed in forming (and maintaining) the tribofilm, and therefore if part of the tribofilm is removed due to the contact, this corresponds to an effective removal of material from the substrate. This principle is the basis of the mild wear model of Bosman & Schipper (Ref (48)), who linked the rate of substrate wear to the rate of tribofilm removal by considering the volumetric percentage of iron as a function of depth in the tribofilm. The functional form was determined from X-ray photoelectron spectroscopy analysis.

In the present work, the link between the substrate wear and the tribofilm takes a different form. The details are explained elsewhere (53) but, in brief, the wear model is a modified version of Archard’s wear equation in which the wear coefficient is related to the local tribofilm thickness. The local wear depth of each point at the surface is given by:

$$\Delta h(x,y) = \frac{K(h)}{H}.P(x,y).\Delta t.v \qquad (2)$$

in which H, $K(h)$, P, v, and Δt are the material hardness, dimensionless Archard's wear coefficient, local contact pressure, sliding speed, and time step respectively. All the parameters in Equation (2) except $K(h)$ are calculated in the contact mechanics simulation. The decrease in the concentration of substrate atoms within the tribofilm as the distance from the substrate/tribofilm interface increases supports the fact that less wear of the substrate occurs if a thicker tribofilm exists. Hence it is assumed that the coefficient of wear is at its maximum for steel-steel contact (i.e. when no tribofilm is present) and at its minimum when the tribofilm has its maximum thickness. Assuming, in addition, a linear variation with tribofilm thickness h, the coefficient of wear is given by:

$$K(h) = K_{steel} - (K_{steel} - K_{min}).\frac{h}{h_{max}} \qquad (3)$$

where $K(h)$ is the coefficient of wear for a substrate covered by a tribofilm with thickness h. K_{steel} and K_{min} are the coefficients of wear for steel and for the maximum ZDDP tribofilm thickness respectively, and h_{max} is the maximum tribofilm thickness. The values of K_{steel} and K_{min} are determined from a single calibration experiment as described in Section 4. Figure 1 shows a flow chart of the numerical model.

3. Experimental setup

The tests were carried out using a Micropitting rig (MPR) which is shown schematically in Figure 2.

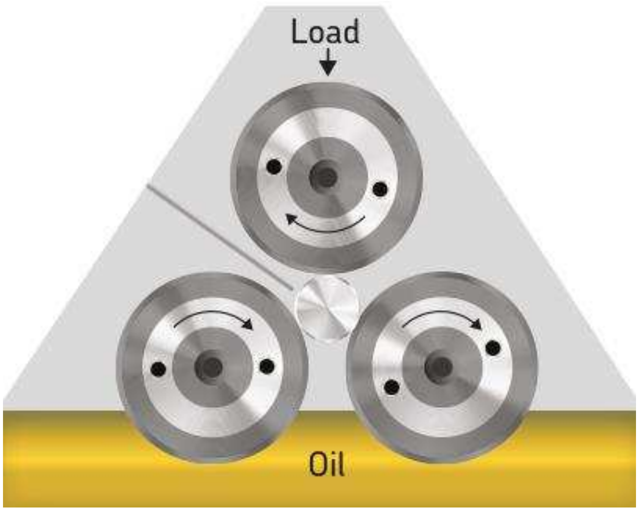

Figure 2. The load unit of the Micropitting Rig (MPR)

The principle part of the Micropitting rig is the load unit which includes a spherical roller 12mm in diameter (taken from a spherical roller bearing), which comes into contact with three larger counterbodies (which are in fact inner rings of a cylindrical roller bearing). The roller and the rings can be ground and/or honed and finished to any desired roughness on the surface. With this configuration, the roller accumulates loading cycles 13.5 times faster than any of the three rings during a test. The oil is carried into the contact by the two bottom rings, creating the conditions of fully lubricated contact – depending, of course, on the desired lubrication regime.

The maximum load that can be applied on the machine is 1250 N, corresponding to a maximum Hertzian pressure of 2.75 GPa, which is high enough for bearing studies. The temperature can be controlled up to 135ºC and the maximum tangential speed is 4 m/s.

The roller and rings are driven by two independent motors, which means that a controlled slide-to-roll ratio of ±200% can be reached. The size of the Hertzian contact varies with the load and the transverse radius of the roller, but the typical values are around 0.244 × 1.016 mm (in the rolling and transverse direction, respectively) corresponding to the maximum Hertzian contact pressure of 1.5 GPa. The operating conditions used in the present work are listed in Table 1. The oil temperature, load, speed and slide-to roll ratio were maintained constant during the experiments. The roughness was changed (on the rings only), to simulate different lubrication conditions.

Over a given experiment duration, the number of rolling cycles experienced is different for the roller and the rings; in fact each cycle of the rings corresponds to 13.5 cycles of the roller.

The lubricant used was a synthetic model oil (poly-alpha-olephine, PAO) mixed with 1% weight of primary zinc dialkyl dithiophosphate (ZDDP). The properties of the oil and additive are listed in Table 2.

Table 1. List of experimental test conditions for the Micropitting rig

Temperature	90ºC
Entrainment speed (U_e)	1 m/s
Slide-to-roll ratio ($\frac{U_s}{U_e}$)	2%
Hertzian contact pressure	1.5 GPa
Lubricants	PAO + ZDDP 1%
Number of cycles for roller	20, 50, 100 kcycles
Number of cycles for rings	1.48, 3.7, 7.4 kcycles
R.M.S. roughness roller	50±10 nm
R.M.S. roughness rings	100±20nm, 200±20nm, 600±50 nm
Value of λ ratio	0.58, 0.3, 0.1

Table 2 Properties of base oil and additive used for experiments.

Code	**Kinematic viscosity 40°C (mm^2/s)**	**Kinematic viscosity 100°C (mm^2/s)**	**Sulphur content (wt%)**	**Phosphorus content (wt%)**
Synthetic Oil	56.2	9.84	0.01	0.00
Primary ZDDP (C_8)	---	---	23.4	11.3

For each roughness value, tests with different running times were carried out in order to obtain the evolution of roughness during the running-in period. In each new test, the roller was replaced with a fresh roller having the same initial roughness (R_q= 50±10nm). The same ring samples were used in each set of experiments (i.e. for a particular roughness), but each time the contact with the roller was at a different, previously unused, position along the width of the rings. The advantage of testing the same ring at different positions along its width is that the variability of the ring surface topography is kept to a minimum. Hence each test within a set of experiments began with a fresh roller/ring surface contact having, as closely as possible, the same initial conditions. Monitoring of the friction coefficient throughout the tests of different duration showed excellent agreement between tests at corresponding times. The whole process was repeated with a fresh set of rollers and rings to assess the reproducibility of the results. The same changes in roughness were observed over time, indicating that the evolution of the surface topography is reproducible, however there were – as expected – differences in the actual r.m.s. values of roughness at corresponding times, which are reflected in the error bars of the figures presented later.

After each test, the samples were cleaned in an ultrasonic bath with petroleum ether for 5 minutes and then the roughness was measured using White Light Interferometry (Wyko NT1100). As shown in other work (50), the presence of a tribofilm can interfere with the measurements of roughness using White Light Interferometry. The roughness of interest is the roughness of the steel surface and to be able to measure it, the tribofilm had to be removed. The technique consisted of covering the wear track with a drop of ethylenediaminetetraacetic acid (EDTA); the EDTA dissolves the tribofilm and then it is removed with a tissue after 20 seconds by just rubbing the wear track. The roughness of each roller sample was accurately measured at 5 different circumferential locations along the contact track. The same process for roughness measurements was repeated for each of the rings and then the roughness r.m.s.value was obtained by averaging all the measured R_q values. Changes in R_q values for the roller and the three rings were monitored with time. Figure 3 shows example roughness profiles.

The morphology of ZDDP-derived reaction layers was observed with a Zeiss Supra 55 scanning electron microscope (SEM) using 5 kV electron beam voltage in the secondary electron mode. Analysis of the chemical composition of the ZDDP-derived tribofilm was made by means of X-ray photoelectron spectroscopy (XPS) using a PHI 5000 Versa Probe Spectrometer (Ulva-PHI Inc, Chanchassen, MN, USA) equipped with a monochromatic Al kα source (1486.6 eV). The data were collected with a beam size of 100 µm and a power of 25W in the FAT analyzer mode. The pass energy was 117.0 eV with energy step size of 1 eV for Survey scan and 46.95 eV with an energy step of 0.1 eV for high resolution spectra. During all the measurements the pressure was always below 10^{-7} Pa.

The identification of the wear track was performed by Scanning X-ray images (SXI) collected in an area of 1×1 mm^2, allowing the identification of the different analysis locations inside the wear track.

<table>
<tr><td colspan="2">Roller</td></tr>
<tr><td>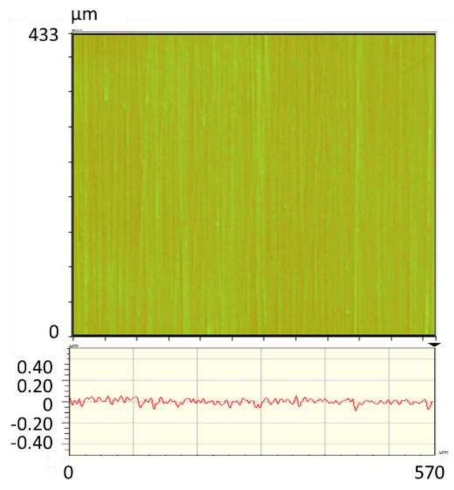
</td><td>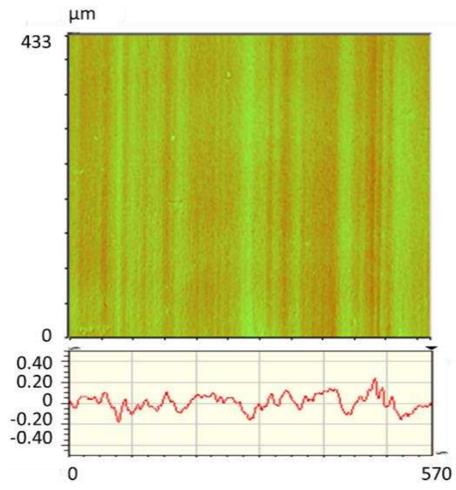
</td></tr>
<tr><td>Initial Surface</td><td>After 100 kcycles</td></tr>
<tr><td colspan="2">Rings</td></tr>
<tr><td>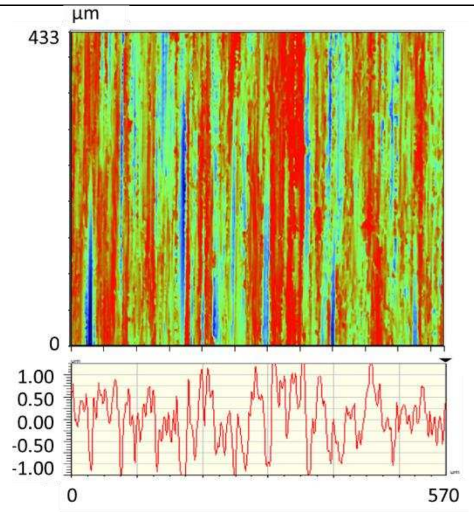
</td><td>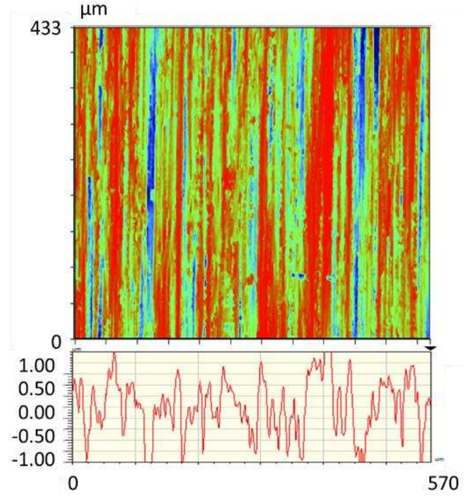
</td></tr>
<tr><td>Initial Surface</td><td>After 7.4 kcycles (of the rings)</td></tr>
</table>

Figure 3. Example of Wyko roughness measurements (all values are in micro metre).

XPS data were processed by using CASA XPS software (version 2.3.16, Casa Software Ltd, UK). The detailed spectra were fitted with Gaussian/Lorentzian curves after linear background subtraction. Charge effect is taken into account by referring to C 1s Binding Energy at 285.0 eV.

The profile of the chemical composition of the ZDDP-derived tribofilm were obtained by using an Ar+ ion gun source with an energy of 2 keV, 2×2 mm^2 area, 10 µA sputter current and 60s of waiting time before spectra acquisition. The sputtering rate for the tribofilm was found to be 4.5 nm/min using optical profilometry and measuring the wear depth after 10 min of sputtering. Sputtering depth profiles were processed by using MultiPack™ Software (version 8.3, ULVAC-PHI Chanchassen, MN, USA), and the reaction layer thickness was defined as the thickness where the atomic concentration of O1s signal is less than 5% for steel samples. The sputtering time provides the measures of layer thickness.

The surface composition and morphology was analyzed by X-ray photoelectron spectroscopy (XPS) and scanning electron microscopy (SEM) coupled with energy-dispersive X-ray spectroscopy (EDX) before roughness measurements.

The specimens used were made of steel AISI 52100 (chemical composition shown in Table 3), with elastic modulus of 210 GPa and a Poisson's ratio of 0.27.

Table 3 Chemical properties of steel AISI 52100 in %

	Cr	**Ni**	**Mn**	**Mo**	**Si**	**C**	**S**	**Cu**
AISI 52100	1.350	0.250	0.450	0.100	0.350	1.050	0.015	0.030

4. Numerical results and discussion

The Micropitting rig (MPR) experiments, the results of which will be discussed in the next section, were simulated with the numerical model. The contact mechanics model was adapted to the same configuration as the MPR. It should be noted that the roughness of the surfaces is characterized by a reasonably large area of the surfaces. Using such large areas as input into numerical model makes it computationally expensive to simulate, especially for the high numbers of loading cycles that result in the evolution of surface topography. In principle, the study area should cover at least several wavelengths of the surface in order to be reasonable. For the surfaces used in this work, an average wavelength of 15 to 20 µm was identified.

Simulations were conducted with different domain sizes to establish the most appropriate size to ensure numerical accuracy while minimizing the computational effort and hence simulation time required. It was found that a computation domain of 64µm×64µm area consisting of 64 nodes of one micron size in each dimension was the minimum domain needed; domain sizes below this were found to be unreliable. This size covers 3-4 roughness ridges, and it is known that at least 3 roughness ridges should be resolved to be able to track the surface topography evolution. To enable simulations over many cycles in a reasonable time, the 64µm×64µm domain was used in all the simulations presented here.

Because of the high number of loading cycles it is not possible to simulate all the loading cycles, even with the smallest appropriate domain size, so numerical experimentation was conducted to optimize the simulation time and the frequency with which the topography was updated. Selection of the size of the wear time-step is dependent on several parameters, the most important of which are the contact pressure, yield stress of the solid, coefficient of wear and the lubrication regime. For this reason it was decided to have finer time-steps in the beginning of the contact, due to higher plastic deformations, and have bigger time steps following that. Hence over the first 100 load cycles, the geometry was updated after every loading cycle. Thereafter the geometry was modified after every 100 loading cycles to increase the time efficiency of the simulations.

The numerical model follows a semi-deterministic approach so that some parameters in the model should be calibrated prior to any predictions. One important calibration parameter is the initial coefficient of wear used in the wear model. To determine this, simulations were run with different initial coefficients of wear and the predicted wear in each case was compared with that observed in one particular experimental test. The initial coefficient of wear giving the closest match with the experiment was then used for the rest of the simulations.

The other important parameters in the model are the tribofilm growth model parameters of Equation 1. These parameters (x_{tribo}, h_{max}, C_3 and C_4) are obtained by fitting the mathematical expression of Equation 1 to experimental tribofilm thickness results. Ideally, for best accuracy, measurements of the tribofilm thickness from specific MPR experiments presented here should be used for calibration. However, this was not possible because the measurement of the tribofilm thickness on the rings and rollers was experimentally cumbersome, and furthermore would have produced insufficient data points to allow fitting of Equation 1. Therefore, in this paper, the calibration parameters are actually the ones reported previously in Ref (52), which were obtained using experimental tribofilm thickness measurement results reported in Naveira Suarez et al. (61). Although that work used a different experimental arrangement, the materials used (Steel AISI 52100 and PAO oil with ZDDP antiwear additive) were the same as those in the present work. Hence the same calibration parameters (presented in Table 4) were used in this work for simplicity.

Inevitably a semi-deterministic model such as the one used here involves a number of parameters that must be determined by reference to experimental data. It is therefore natural to ask: what is the sensitivity of the model to the values of these parameters, and how can such parameters be determined in the absence of experimental data? Importantly, in the results presented here, two key elements of the model, namely the initial specific topography of the surfaces and the tribofilm formation parameters, were effectively obtained independently of the MPR experiments. For the tribofilm parameters (x_{tribo}, h_{max}, C_3 and C_4), values from a different study using the same materials but different configuration were used. For the surface topography, artificial surfaces were created with roughness and lateral asperity size matching the experiments. Indeed, the model of equation (1) has been adapted to the pool of experimental results available in the literature, to provide a good indication of the range of the parameters and to allow selection of a reasonable set of calibration parameters in the absence of specific experimental data (see Ref (62)).

Table 4 The calibration parameters

Parameter	Value	Description
K_{steel}/H	1.25×10^{-17}	Dimensional wear coefficient for steel (m^3/Nm)
K_{min}/H	1.25×10^{-18}	Dimensional wear coefficient for maximum film thickness (m^3/Nm)
h_{max}	176	Maximum local tribofilm thickness in the formation process (nm)
x_{tribo}	4.13×10^{-16}	Tribofilm formation rate constant
C_3	0.1125	Tribofilm removal constant
C_4	0.0006799	Tribofilm removal exponential factor
E_1, E_2	209	Young's modulus of two surfaces (GPa)
ν_1, ν_2	0.3	Poisson's ratio
H_{steel}	8	Hardness of the steel substrate (GPa)
H_{tr}	2	Hardness of the tribofilm at steady state tribofilm thickness (GPa)

The growth of the tribofilm is assumed to occur only at contacting asperities. Therefore the local contact properties calculated from the contact model are responsible for the formation of the tribofilm at the asperity scale. It is observed experimentally that the formation of the tribofilm on asperities can lead to change in the mechanical properties of interfaces and also results in an increase in load-carrying capacities of the contacting bodies (63). The tribofilm has been reported as a solid-like material with different mechanical properties from the substrate (64-66). The difference in the mechanical properties of ZDDP tribofilm at different areas in the bulk was related to the different chain lengths of polyphosphate, with shorter polyphosphates being present deeper in the tribofilm and longer chains existing close to the surface of the film (67-70). In the current model, the values of the tribofilm hardness at the surface and near the substrate can be approximated from experimental results (71). This variation is assumed to be between 2 and 6 GPa, changing linearly from the surface to the substrate. This is a gross assumption but, given the lack of experimental data on the specific form of this variation, it seems reasonable. In addition, the elastic properties of the tribofilm also vary from the surface to the bulk and this variation is related to hardness variations (72).

Once the tribofilm, which is a solid–like material, forms on the contact asperities, the topography of the surfaces is changed and the contact conditions between surfaces may change as a result. This change in the contact conditions can lead to a different topographical evolution at the interface in comparison to the case when no such tribofilm is formed. This effect can be seen in the numerical results.

One example of the model results is shown in Figure 4. It can be seen that the rougher surface (Figure 4 (a) left) starts to become smoother in the beginning of the contact then gradually becomes rougher over time. It can be interpreted that in the beginning of the contact the dominant plastic deformation can lead to relatively fast surface deformations. The tribofilm formed on the surfaces will change the local mechanical properties of the surfaces as well as their micro-geometry. An increase in the roughness of the rougher surface can occur because of the growth of the tribofilm, which is a solid-like material. Fast growth of the tribofilm on the highest asperities in the running-in stage changes the geometry of those asperities in the contact. The new asperity consists of a substrate (steel) and the glassy polyphosphate tribofilm on top, which is a solid-like material. It can come into contact with the counterbody and increase the average peak-to-valley height difference. The counter body also consists of a tribofilm on top but, in the running-in stage, there are numerous asperities that are not covered by the tribofilm yet. This will lead to the contact of the high asperities consisting of tribofilm into the asperities of the counterbody that are not yet covered by the tribofilm. After some time, the surface becomes gradually smoother because of the mild wear occurring at the contacting asperities. Different stages of the simulation are numbered in Figure 4. Point 0 is the beginning of the simulation where the initial surfaces are not in contact yet. Point 1 is the time after 20 kcycles of the roller. It is the time by which the highest asperities of the surfaces are plastically deformed. Point 2 is selected to be the end of the experiments (after 100 kcycles of the roller). These points are selected and indicated in Figure 4 as reference times that are used in Figure 5 and Figure 6 to study the difference in the surface topography and tribofilm formation, respectively, at different times of the simulation. Note that the number of cycles for the ring and the roller are different at Points 1 and 2, and therefore the horizontal axis scales are different in Figure 4-a and Figure 4-b, but these points correspond to the same physical time.

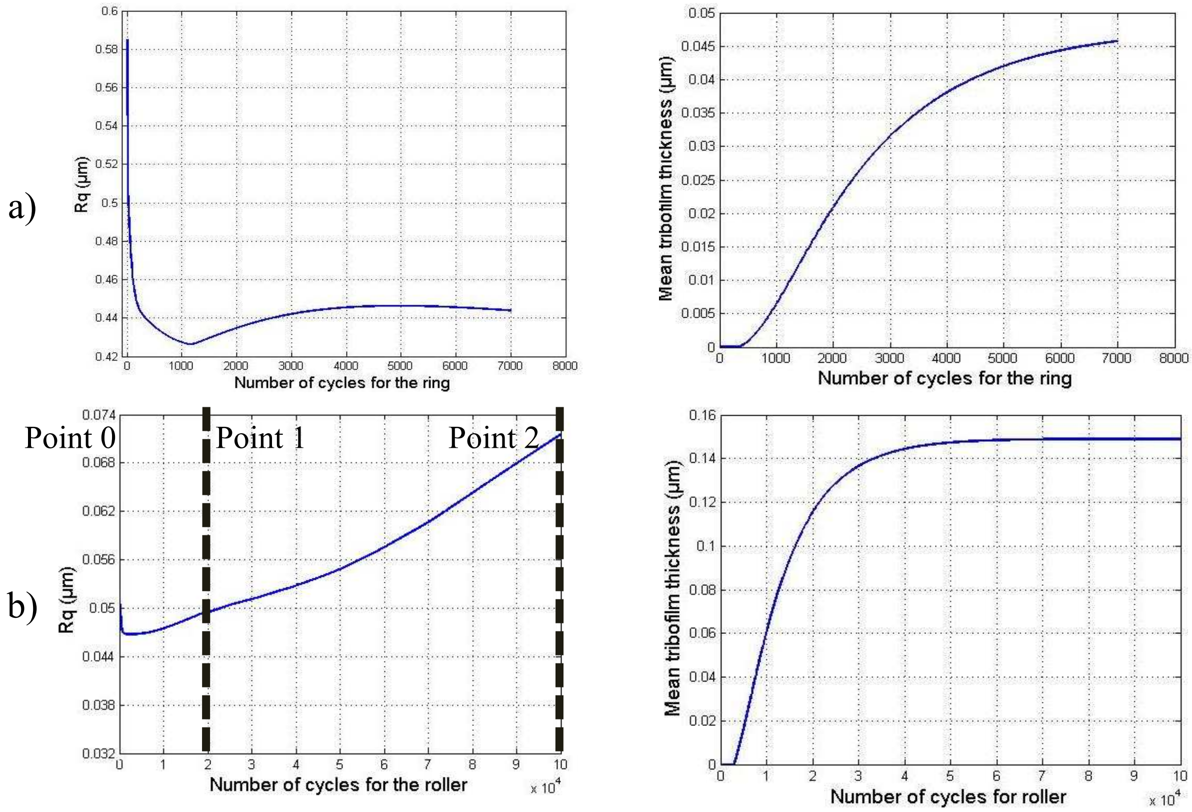

Figure 4 (Left) Roughness evolutions and (Right) tribofilm build up for the (a) rougher (ring) and (b) smoother (roller) body as predicted by the model, for the case of initial ring roughness 600 nm.

In the beginning of the contact, the highest asperities of the rough surface experience high levels of plastic deformation, which results in smoothing of the rough surface. Simulation results to confirm this are shown in Figure 5. It can be seen in the figure that the asperities of the initial surface (Figure 5-a) are smoothed (Figure 5-b) after 20 kcycles of the roller. The asperities are then smoothed further due to mild wear (Figure 5-c). On the other hand, contact between the smooth surface and the highest asperities of the rough surface produces indentations in the smooth surface (Figure 5d-f). Growth of the tribofilm on the contacting asperities then results in roughening of the rough surface. The simulation results of the inhomogeneous tribofilm formed on the surface confirms this and the results are shown in Figure 6. It can be seen that the tribofilm grows on the contacting asperities both in thickness and coverage.

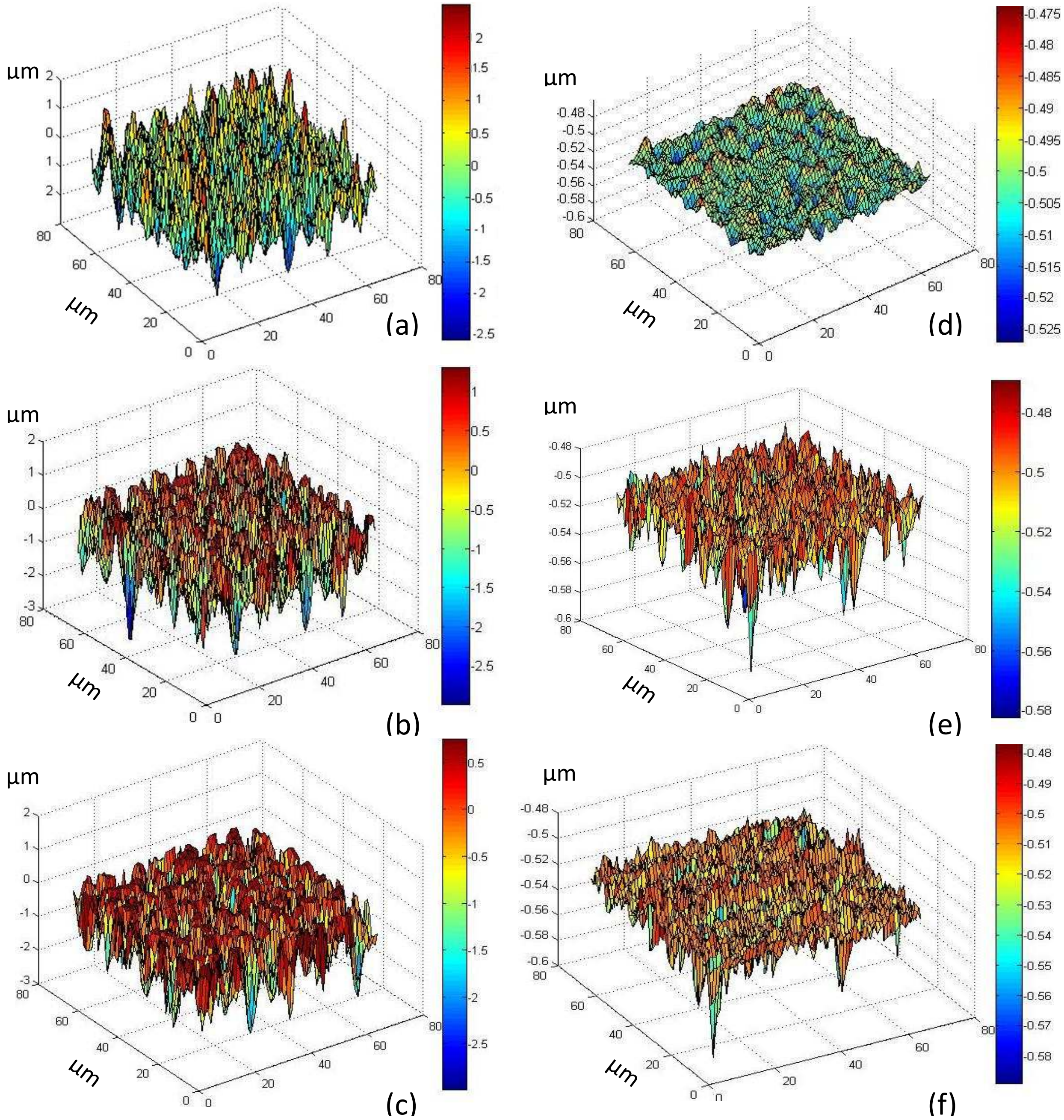

Figure 5 Surface topography evolution predicted by the model (a) surface of the ring before the experiment point 0 (b) surface of the ring at point 1 (c) surface of the ring at point 2 (d) surface of the roller before the experiment point 0 (e) surface of the roller at point 1 (f) surface of the roller at point 2

This growth of the tribofilm is responsible for the increase in the roughness of the ring. The growth of the tribofilm on both rough (ring) and smooth (roller) surfaces are shown in Figure 6. It can be seen that the growth on the roller (smooth surface) is faster in comparison to the ring (rough surface), since the roller experiences 13.5 times more loading cycles in a given time period and the growth of the tribofilm on the surfaces is directly proportional to the time of rubbing.

The smoother body (roller) experiences a relatively fast initial decrease in the roughness value (see Figure 4). The root mean square sharply decreases from 0.05 µm to about 0.047 µm; this is because of high plastic deformation and decrease in the height of the highest peaks on the smooth surface. Then an overall increase in the roughness of the smoother surface is observed because of contact with a rougher surface and also fast growth of the tribofilm. Similar results were obtained in (50). It should be noted that the tribofilm is formed on both surfaces and the corresponding average tribofilm thickness is shown in Figure 4 parallel to the roughness evolution of both surfaces for comparison purposes. The next section describes the results of experiments carried out to validate the model and to confirm its predictions of the changes in the topography of the surfaces.

5. Experimental results

The roughness evolution of the MPR roller and the three different rings obtained by the method described in Section 3 is shown in Figure 7. The figure shows that when the roughness of the rings is higher, longer running-in will occur which delays the tribofilm build up and the surface modifications at the beginning are very similar to those found without the presence of additives. With smoother surfaces, the roughness modifications decrease because of the formation of a tribofilm. When the contact is in the EHL regime ($R_{q\,\mathrm{rings}}$=100 nm), the process is mainly governed by the coverage of the contacting asperities with ZDDP tribofilm. The asperities of the bodies covered with a tribofilm promote the roughening of the ring's surface until it reaches the steady state. This can be noticed because the differences in roughness are not visible during the initial cycles on the smoother body. It is clear that, when the contact is in the boundary or mixed lubrication regimes ($R_{q\,\mathrm{rings}}$=600 nm and $R_{q\,\mathrm{rings}}$=200 nm, respectively), the first process which occurs on the surface is the plastic deformation of asperities, leading to a smoothing of the surface and this is in agreement with the numerical results reported in Section 4. In complete boundary lubricated contact ($R_{q\,\mathrm{rings}}$=600 nm), after the plastic deformation process, the tribofilm can increase the roughness of the surfaces.

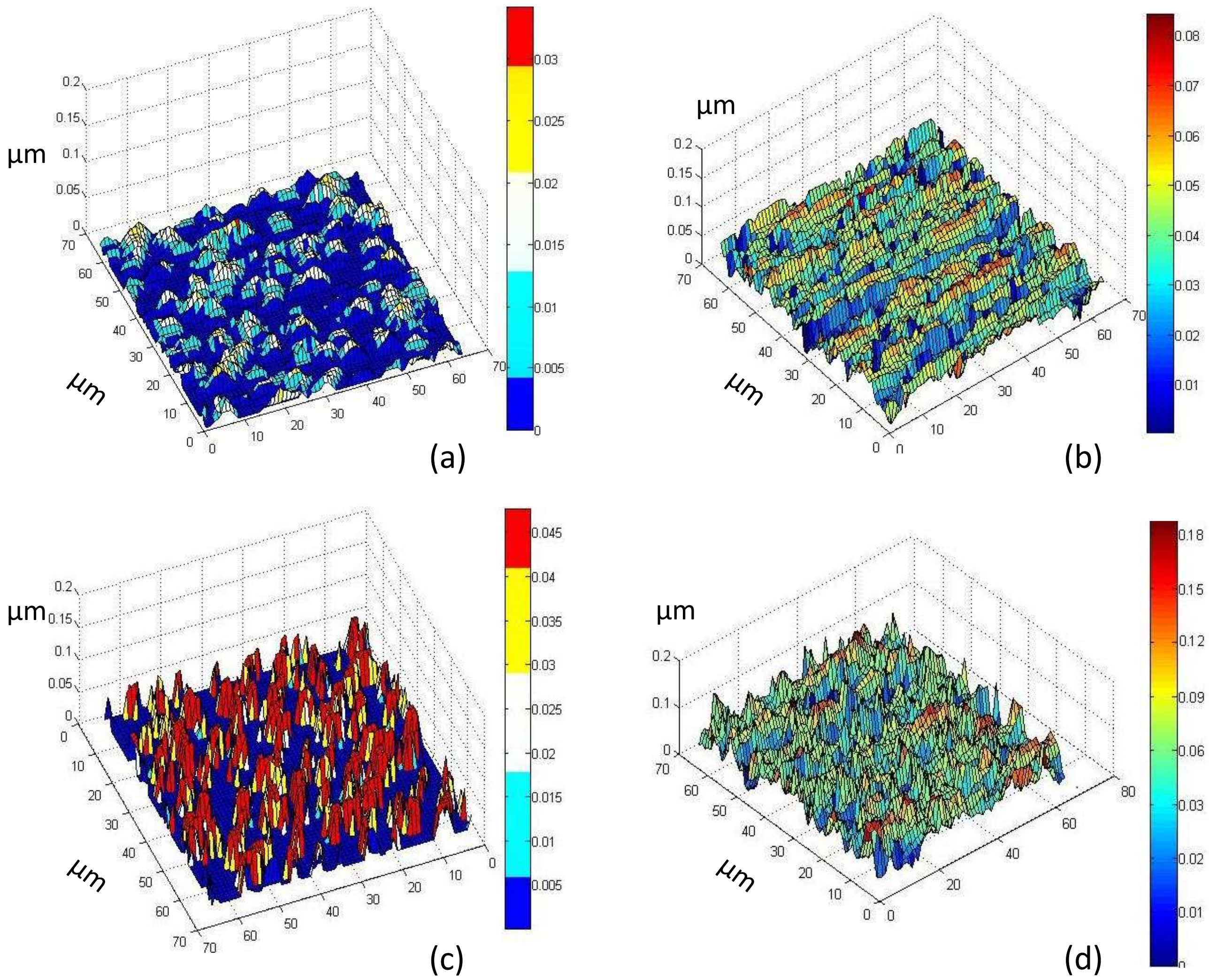

Figure 6 Tribofilm growth on the contacting asperities (a) at point 1 for rough surface (ring) (b) at point 2 for rough surface (ring) (c) at point 1 for smooth surface (d) at point 2 for smooth surface

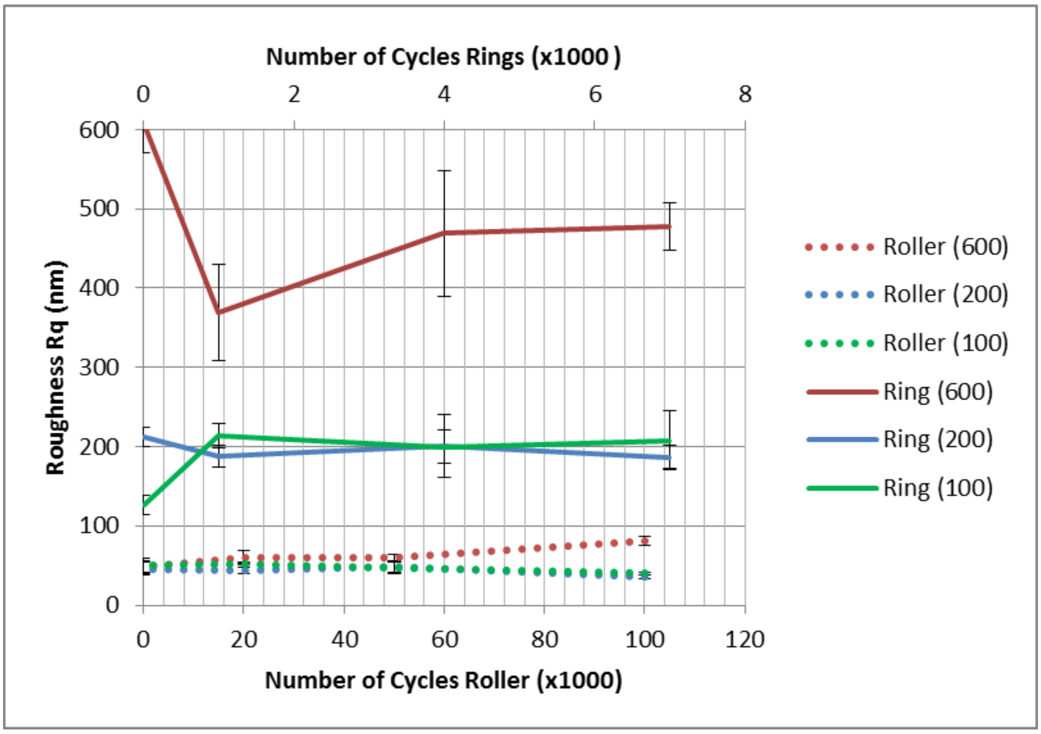

Figure 7 Experimental results on different roughness of rings

The numerical model is only valid for boundary lubrication conditions. Therefore, for validation purposes, it was necessary to compare numerical results with the experiments in boundary lubrication regime. Although this is one of the shortcomings of the numerical framework, it is important to develop robust models in boundary lubrication that are able to capture tribochemistry phenomena. The experimental topography measurements for the case of boundary lubrication ($R_{q\,\mathrm{rings}}$=600 nm), are shown in Figure 8 for comparison purposes. Good qualitative agreement is seen between the experimental (Figure 8) and the model (Figure 4) results. It is demonstrated in the model that the roughness of both smooth and rough contacting surfaces will converge to specific values but they will never reach the same number (see also (50)). It was also shown that different surface roughness configurations would have different topography behaviour. The initial roughnesses of both contacting surfaces are the key parameters which govern the further roughness evolution. It was assumed in the numerical results of Section 4 that the tribofilm growth on the contacting asperities is responsible for the roughening of the rings. The numerical results for tribofilm growth were then presented in the same section. To confirm this by means of experimental data, surface analysis results of the tribofilm formed on the surface are reported here.

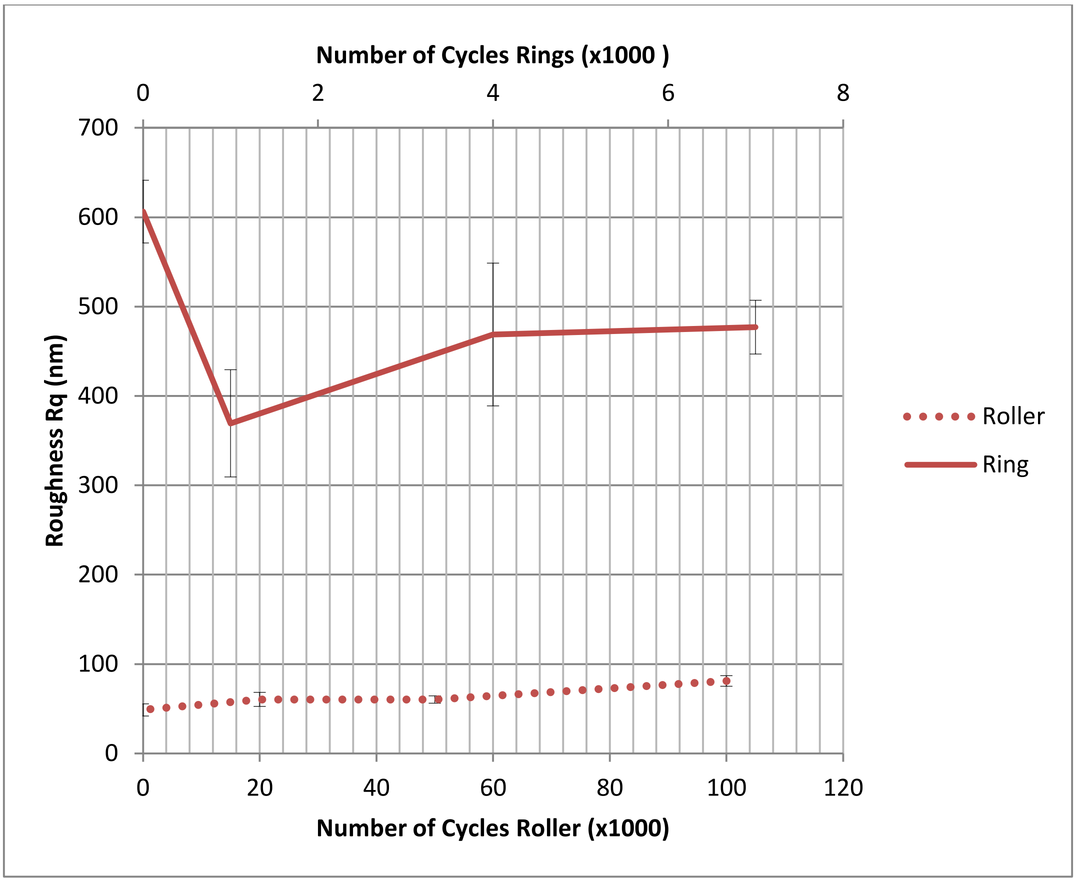

Figure 8 Roughness measurement experimental results for both ring and roller

Figure 9 shows an SEM image of the tribofilm in the middle of the wear track formed on the roller. It can be seen from the image how the tribofilm is formed on the wear track due to severe conditions. It can be compared to the numerical results of Figure 6 and a similar pattern can be observed. The image is taken at the end of the experiment in the boundary lubrication regime when the initial roughness of the ring was $R_{q\,\mathrm{rings}}$=600 nm.

XPS analysis performed on the tribofilm showed the oxygen signal with two different peaks. According to the literature, these peaks belong to two different oxygen types: the main peak at 531.6 eV is assigned to the non-bridging oxygen (NBO) in poly(thio)-phosphate chains and also to other oxygen-containing groups such as sulphates, carbonates or hydroxides (73); the second peak at 532.8 eV can be assigned to the presence of the bridging oxygen (BO) which corresponds to P-O-P and P-O-C bonds (73). The P 2p signal was detected at 133.4 eV while the Zn 3s at 140.0 eV. S 2p signal was found on the surface at 161.8 eV which is attributed to the oxidation state of -2 as found in sulphides (74) and thiolates (75) or when sulphur is substituting oxygen atoms in a phosphate (73).

Figure 10 shows the XPS depth profile of the tribofilm formed on the surface of the ring in the boundary lubrication regime. The thickness of the tribofilm was found to be about 55 nm, which is consistent with the prediction of the numerical model (see Figure 4 (a), right). According to previous studies (68), the tribofilm is composed of phosphate chains, the length of which can be determined by the ratio between bridging oxygen and non-bridging oxygen (76). As Figure 11 shows, in this case, the ratio is approximately 0.25, which corresponds to the presence of polyphosphate chains, i.e. chains of more than 3 phosphate groups (76, 77). A similar value of the ratio was also obtained for the mixed lubrication regime. The polyphosphate chain length influences the local mechanical properties of the tribofilm on the surface, and different mechanical behaviour such as the durability of the films (63-65, 78). For this reason, the chemical characteristics of the film are important parameters in defining the physical and mechanical behaviour of the film and the corresponding changes in the topography of the surfaces. The surface analysis results shown in Figure 9 and Figure 10 indicate that the tribofilm covers the surface asperities of the roller. In the numerical simulation results of Section 4, growth of such a tribofilm was reported to be the reason for the increase of roughness of the ring surface.

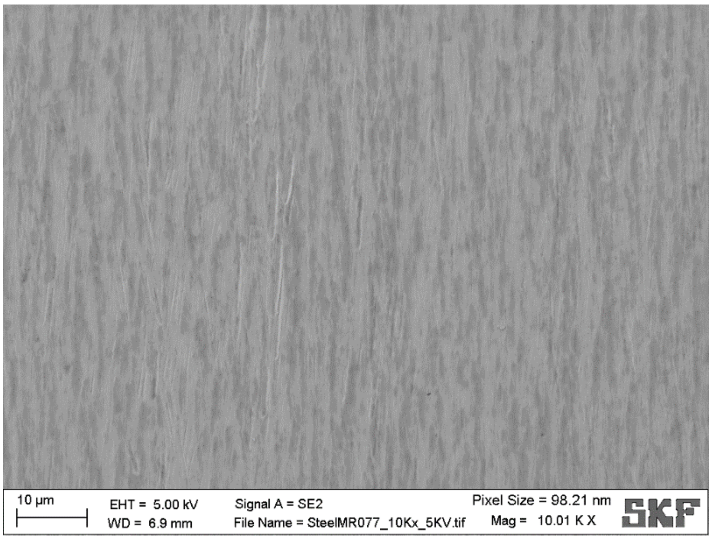

Figure 9 SEM image of the tribofilm formed on the wear track

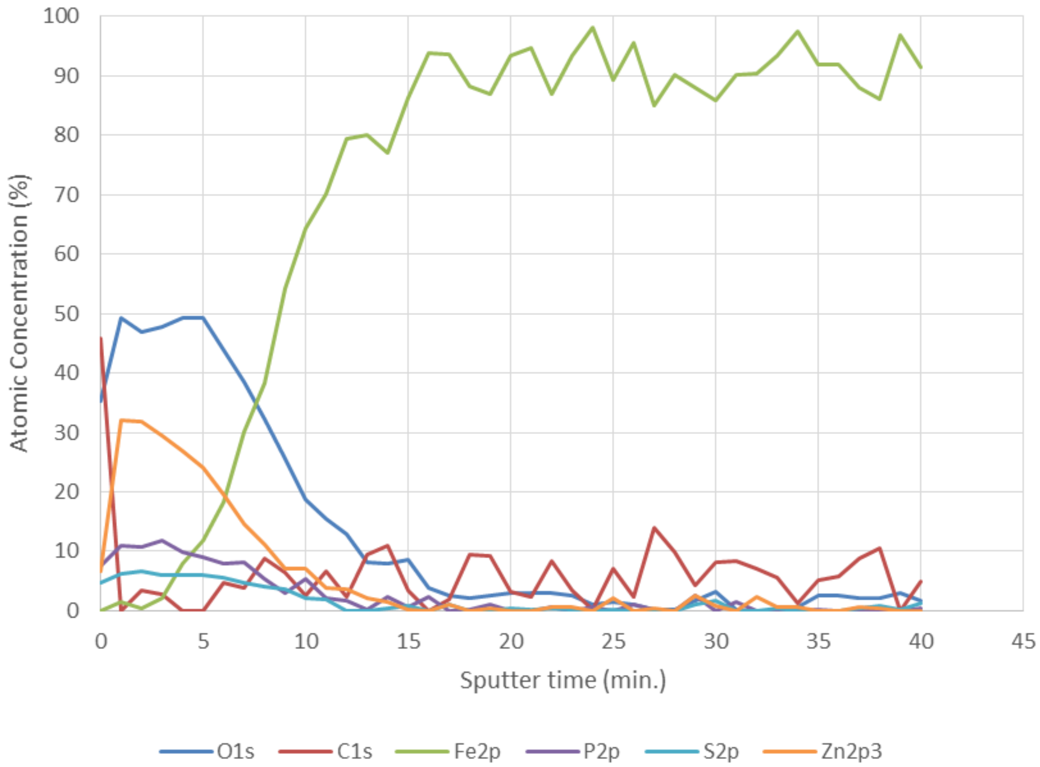

Figure 10 XPS depth profile of the tribofilm formed on the surface of the ring

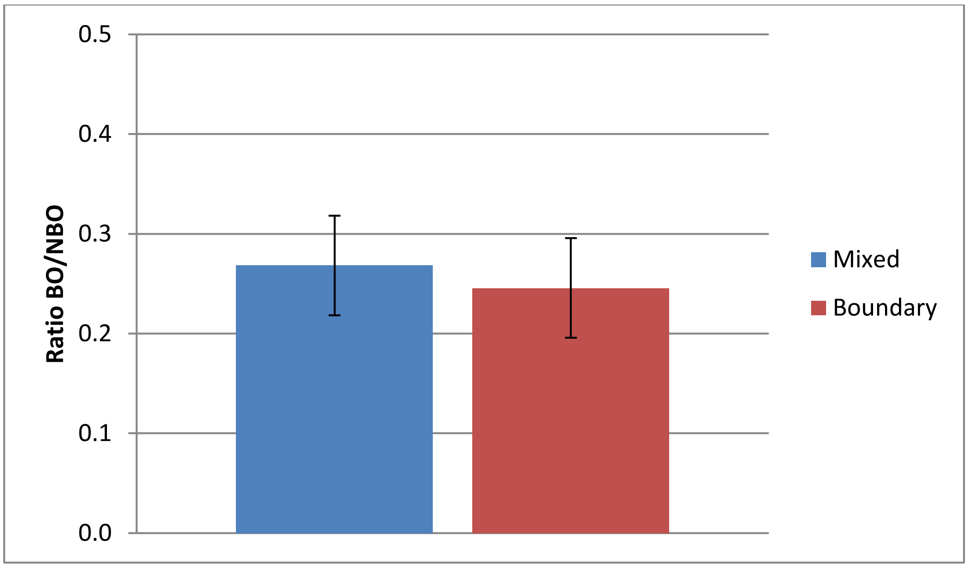

Figure 11. Ratio BO/NBO for the two lubricating conditions

6. Effect of load on surface topography evolution

Having been validated against the experimental measurements, the numerical model can be used to conduct wider parametric studies to explore the influence of important factors such as contact load and material hardness on the evolution of the surface topography. To illustrate, simulations were carried out for different contact loads to see the effect on the roughness evolution of the rings with initial roughness 600 nm. The results are shown in Figure 12. The selected contact pressures were between 700 MPa and 2 GPa in order to see the effect of a relatively wide range of loads. It should be noted that even with the lowest load the λ ratio was small enough that the contact was in the boundary lubrication regime.

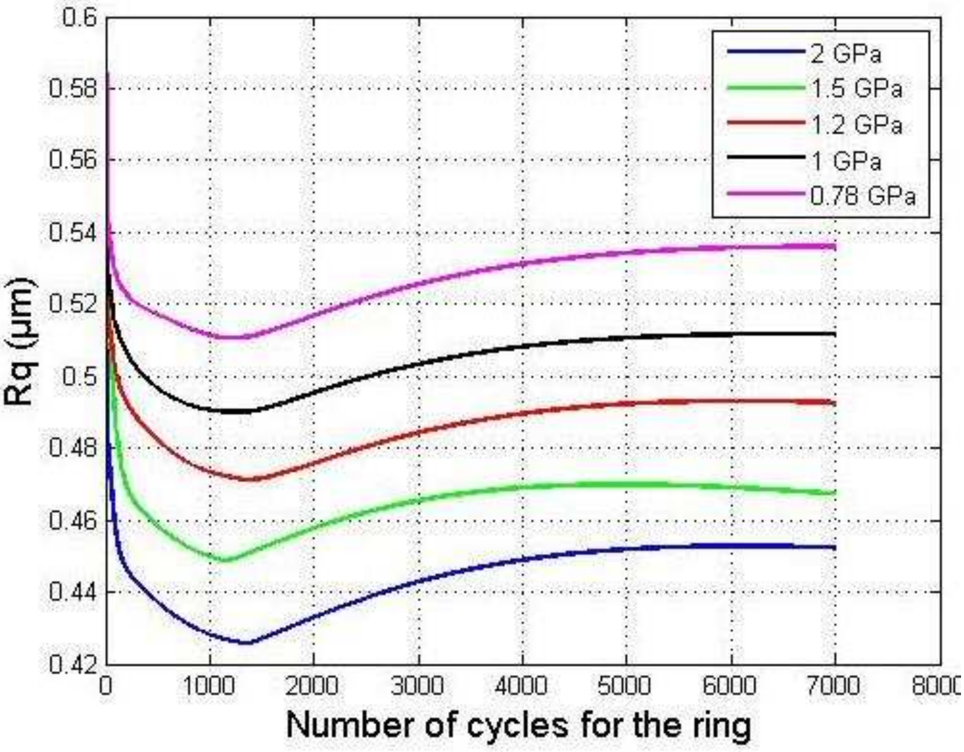

Figure 12 Simulation of roughness evolution of the rings at different contact loads

In this specific contact configuration, it is observed that the higher loads change the surface roughness more than the lower loads, which is consistent with the expected higher plastic deformation. Clearly the load does influence the evolution of the surface roughness, but the differences in the magnitude of plastic deformation are not significant as can be seen from the results in Figure 12. For instance, doubling the contact pressure from 1 to 2 GPa results in a difference in roughness of around 60 nm, or about 12%, at 7000 cycles of the rings. The same pattern in results were reported by Wang et al (79) and also confirmed by Jamari (80).

7. Effect of surface hardness on topography evolution

Simulations have been also carried out for different material hardnesses and the results are shown in Figure 13. The hardness of the contacting bodies influences the elastic-plastic behaviour and directly affects the time changes in the surface topography. Because the contact code formulation was developed for similar materials, the hardness mentioned here was the hardness of both contacting surfaces. In this study, the hardness variation was from 4 GPa to 12 GPa. It can be seen from the results that the harder materials experienced less plastic deformation and also less variation in topography due to either plasticity or wear. As mentioned in the numerical model of Section 2, the material hardness is the criterion for plastic flow. Higher hardness results in less plastic deformation of the surfaces and it consequently results in less change in the topography. Softer materials are more likely to deform and experience larger variations in topography. In addition, based on the formulation of Archard's wear equation, harder materials are less prone to wear (see equation 2).

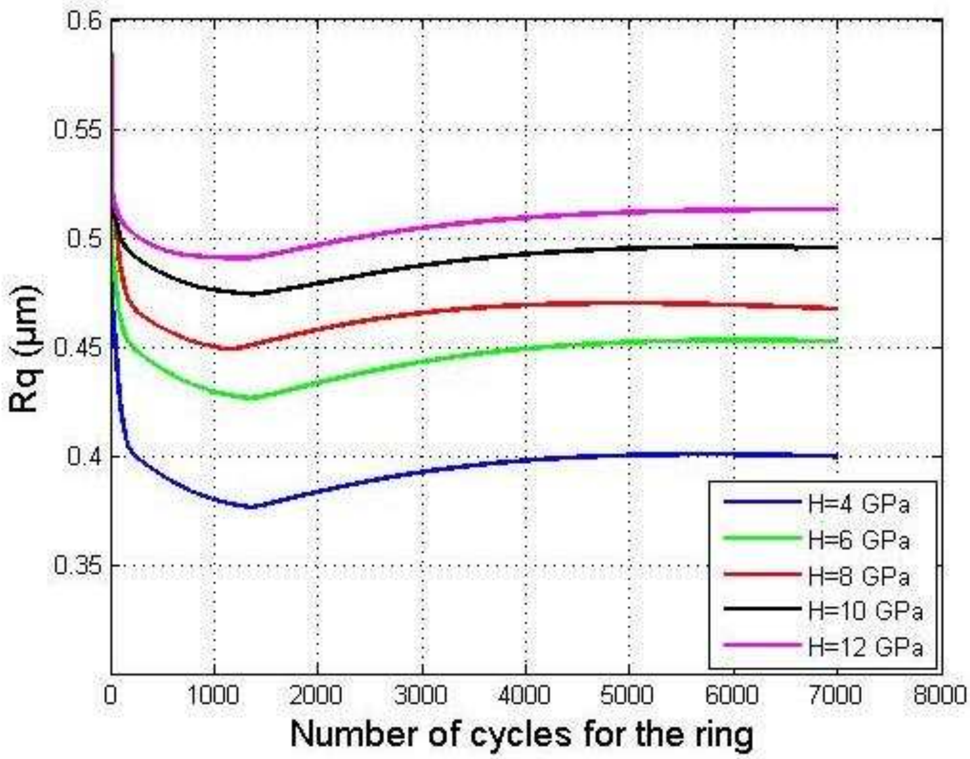

Figure 13 Simulation of roughness evolution for materials of different hardnesses

8. Conclusions

- The predictions of the emerging topography were validated against experiments carried out using a Micropitting rig. The surface topography is affected by surface plastic deformations, tribofilm growth and wear. It is shown that during initial contact, high plastic deformations on the surfaces are responsible for rapid initial changes in the topography.
- Results also show that growth of a tribofilm can change the local mechanical properties at interfaces which can influence the further roughness evolution of the surfaces. One interesting conclusion from an analysis of the pool of numerical simulations is that the

roughness evolution of both contacting bodies is significantly influenced by the initial roughness patterns. It means that the initial roughness of both surfaces in combination will determine the mode of topography evolution and hence a proper finishing of both contacting surfaces is required to obtain a better tribological performance in the steady-state.

- The growth of polyphosphate tribofilm formed on the contacting asperities is responsible for an increase in the roughness of the surfaces in contact. This was shown numerically (in Section 4) and verified with experimental measurements (Section 5) of roughness (after removal of the tribofilm). Experimental surface analysis also showed that a tribofilm was formed on the surface with a thickness very close to the predicted values.
- Clearly a model is more general and more useful if it is able to predict the key behaviour of a system without having to rely on very specific details and measurements of individual experiments. Therefore the good qualitative agreement between the predicted behaviour of the system and the experimental observations is very encouraging.

9. Acknowledgements

This study was funded by the FP7 program through the Marie Curie Initial Training Network (MC-ITN) entitled “ENTICE - Engineering Tribochemistry and Interfaces with a Focus on the Internal Combustion Engine” [290077] and was carried out at the University of Leeds and the SKF Engineering & Research Centre in the Netherlands. The authors thank all ENTICE partners for useful discussions on the topic and the methodology.

References

1. Blau PJ. On the nature of running-in. Tribology International. 2006;38(11):1007-12.
2. Blau PJ. Running-in: Art or engineering? Journal of materials engineering. 1991;13(1):47-53.
3. Atala H, Rowe G. Surface roughness changes during rolling. Wear. 1975;32(2):249-68.
4. Masouros G, Dimarogonas A, Lefas K. A model for wear and surface roughness transients during the running-in of bearings. Wear. 1977;45(3):375-82.
5. Dong W, Stout K. An integrated approach to the characterization of surface wear i: Qualitative characterization. Wear. 1995;181:700-16.
6. Jeng YR, Lin ZW, Shyu SH. Changes of surface topography during running-in process. Journal of tribology. 2004;126(3):620-5.
7. Karpinska A. Running-in and the evolution of metallic surfaces subjected to sliding and rolling contact: Imperial College London; 2010.
8. Chou C, Lin J. Tribological effects of roughness and running-in on oil-lubricated line contacts. Proceedings of the Institution of Mechanical Engineers, Part J: Journal of Engineering Tribology. 1997;211(3):209-22.
9. Tyagi MR, Sethuramiah A. Asperity level conformity in partial EHL. Part I: Its characterization. Wear. 1996;1(197):89-97.
10. Sreenath A, Raman N. Mechanism of smoothing of cylinder liner surface during running-in. TRIBOLOGY international. 1976;9(2):55-62.
11. Sreenath A, Raman N. Running-in wear of a compression ignition engine: factors influencing the conformance between cylinder liner and piston rings. Wear. 1976;38(2):271-89.
12. Neale MJ. The tribology handbook: Butterworth-Heinemann; 1995.
13. Goepfert O, Ampuero J, Pahud P, Boving H. Surface roughness evolution of ball bearing components. Tribology transactions. 2000;43(2):275-80.
14. Tripp J, Ioannides E, editors. Effects of surface roughness on rolling bearing life. Japan International Tribology Conference II; 1990.
15. Nélias D, Dumont M, Champiot F, Vincent A, Girodin D, Fougeres R, et al. Role of inclusions, surface roughness and operating conditions on rolling contact fatigue. Journal of tribology. 1999;121(2):240-51.
16. Meng H, Ludema K. Wear models and predictive equations: their form and content. Wear. 1995;181:443-57.
17. Meng H-C. Wear modeling: evaluation and categorization of wear models. 1994.
18. Suh NP. An overview of the delamination theory of wear. Wear. 1977;44(1):1-16.
19. Rabinowicz E. Friction and wear of materials. 1965.
20. Archard J. Contact and rubbing of flat surfaces. Journal of applied physics. 1953;24(8):981-8.
21. Holm R, Holm EA. Electric contacts. 1967.
22. Stachowiak G, Stachowiak G. The effects of particle characteristics on three-body abrasive wear. Wear. 2001;249(3):201-7.
23. Dwyer-Joyce R. Predicting the abrasive wear of ball bearings by lubricant debris. Wear. 1999;233:692-701.
24. Dwyer-Joyce R, Sayles R, Ioannides E. An investigation into the mechanisms of closed three-body abrasive wear. Wear. 1994;175(1):133-42.
25. Godet M. The third-body approach: a mechanical view of wear. Wear. 1984;100(1):437-52.
26. Rabinowicz E, Dunn L, Russell P. A study of abrasive wear under three-body conditions. Wear. 1961;4(5):345-55.
27. Williams J, Hyncica A. Mechanisms of abrasive wear in lubricated contacts. Wear. 1992;152(1):57-74.
28. Olofsson UA, Sören Björklund, Stefan. Simulation of mild wear in boundary lubricated spherical roller thrust bearings. Wear. 2000;241(2):180-5.

29. Olofsson U, Dizdar S. Surface analysis of boundary-lubricated spherical roller thrust bearings. Wear. 1998;215(1):156-64.
30. Ulf Olofsson SrA, Stefan Bjorklund. Simulation of mild wear in boundary lubricated spherical roller thrust bearings. Wear. 2000;241(2):180-5.
31. Flodin A. Wear of spur and helical gears. Royal Institute of Technology, Stockholm, Doctoral Thesis. 2000.
32. Andersson S, Olofsson U, editors. Towards a general model for wear simulation. IRG-OECD Meeting, Uppsala, Sweden; 2005.
33. Andersson S, Söderberg A, Olofsson U. A random wear model for the interaction between a rough and a smooth surface. Wear. 2008;264(9):763-9.
34. E.M. Bortoleto ACR, V.Seriacopi,F.J.Profito,D.C.Zachariadis,I.F.Machado,, A. Sinatora RMS. Experimental and numerical analysis of dry contact in the pin on disc test. Wear. 2012;301(1):19-26.
35. Priit Podra SA. Simulating sliding wear with finite element method. Tribology international. 1999;32(2):71-81.
36. Öqvist M. Numerical simulations of mild wear using updated geometry with different step size approaches. wear. 2001;249(1):6-11.
37. V Hegadekatte NHaOK. Finite element based simulation of dry sliding wear. modelling and simulation in materials science and engineering. 2005;13(1):57.
38. V. Hegadekatte S. Kurzenha NH, O. Kraft. A predictive modeling scheme for wear in tribometers. Tribology international. 2008;41(11):1020-31.
39. V. Hegadekatte J. Hilgertb OKNH. Multi time scale simulations for wear prediction in micro-gears. Wear. 2010;268(1):316-24.
40. Bosman R, Schipper DJ. Running-in of systems protected by additive-rich oils. Tribology Letters. 2011;41(1):263-82.
41. G.K. Sfantos MHA. Wear simulation using an incremental sliding Boundary Element Method. Wear. 2006;260(9):1119-28.
42. Sfantos G, Aliabadi M. A boundary element formulation for three-dimensional sliding wear simulation. Wear. 2007;262(5):672-83.
43. Ilincic S, Vernes A, Vorlaufer G, Hunger H, Dörr N, Franek F. Numerical estimation of wear in reciprocating tribological experiments. Proceedings of the Institution of Mechanical Engineers, Part J: Journal of Engineering Tribology. 2013;227(5):510-9.
44. Ilincic S, Vorlaufer G, Fotiu P, Vernes A, Franek F. Combined finite element-boundary element method modelling of elastic multi-asperity contacts. Proceedings of the Institution of Mechanical Engineers, Part J: Journal of Engineering Tribology. 2009;223(5):767-76.
45. Ilincic S, Tungkunagorn N, Vernes A, Vorlaufer G, Fotiu P, Franek F. Finite and boundary element method contact mechanics on rough, artificial hip joints. Proceedings of the Institution of Mechanical Engineers, Part J: Journal of Engineering Tribology. 2011;225(11):1081-91.
46. Andersson J. Modelling of wear and tribofilm growth. 2012.
47. J. Andersson AA, R. Larsson. Numerical simulation of a wear experiment. Wear. 2011;271(11):2947-52.
48. Bosman R, Schipper DJ. Mild Wear Prediction of Boundary-Lubricated Contacts. Tribology Letters. 2011;42(2):169-78.
49. Joel Andersson, Roland Larsson, Andreas Almqvist, Grahnb M, Minami I. Semi-deterministic chemo-mechanical model of boundary lubrication. faraday Discussions. 2012;156(1):343-60.
50. Morales-Espejel G, Brizmer V, Piras E. Roughness evolution in mixed lubrication condition due to mild wear. Proceedings of the Institution of Mechanical Engineers, Part J: Journal of Engineering Tribology. 2015:1350650115577404.
51. Morales-Espejel GE, Brizmer V. Micropitting modelling in rolling–sliding contacts: Application to rolling bearings. tribology transactions. 2011;54(4):625-43.
52. Ghanbarzadeh A, Wilson M, Morina A, Dowson D, Neville A. Development of a New Mechano-Chemical Model in Boundary Lubrication. Tribology International. 2016;93:573-82.

53. Ghanbarzadeh A, Parsaeian P, Morina A, Wilson MC, van Eijk MC, Nedelcu I, et al. A Semi-deterministic Wear Model Considering the Effect of Zinc Dialkyl Dithiophosphate Tribofilm. Tribology Letters. 2016;61(1):1-15.
54. Tonder YZHaK. Simulation of 3-D random rough surface by 2-D digital filter and Fourier analysis. International journal of machine tools and manufacture. 1992;32(1):83-90.
55. Xuefeng Tian BB. A Numerical Three-Dimensional Model for the Contact of Rough Surfaces by Variational Principle. 1996.
56. F Sahlin RL, A Almqvist, P M Lugt and P Marklund. A mixed lubrication model incorporating measured surface topography. Part 1: theory of flow factors. Proceedings of the Institution of Mechanical Engineers, Part J: Journal of Engineering Tribology. 2009;224(4):335-51.
57. Blok H. The flash temperature concept. Wear. 1963;6(6):483-94.
58. Kennedy F. Frictional heating and contact temperatures. Modern tribology handbook. 2001;1:235-59.
59. Tian X, Kennedy FE. Maximum and average flash temperatures in sliding contacts. Journal of Tribology. 1994;116(1):167-74.
60. Gosvami N, Bares J, Mangolini F, Konicek A, Yablon D, Carpick R. Mechanisms of antiwear tribofilm growth revealed in situ by single-asperity sliding contacts. Science. 2015;348(6230):102-6.
61. Naveira-Suarez A, Tomala A, Pasaribu R, Larsson R, Gebeshuber IC. Evolution of ZDDP-derived reaction layer morphology with rubbing time. Scanning. 2010;32(5):294-303.
62. Ghanbarzadeh A. Mechano-Chemical Modelling of Boundary Lubrication. UK: University of Leeds; 2016.
63. Aktary M, McDermott MT, McAlpine GA. Morphology and nanomechanical properties of ZDDP antiwear films as a function of tribological contact time. Tribology letters. 2002;12(3):155-62.
64. Gabi Nehme RM, Pranesh B. Aswath,. Effect of contact load and lubricant volume on the properties of tribofilms formed under boundary lubrication in a fully formulated oil under extreme load conditions. Wear. 2010;268(9):1129-47.
65. Ramoun Mourhatch PA. Tribological behavior and nature of tribofilms generated from fluorinated ZDDP in comparison to ZDDP under extreme pressure conditions—Part II: Morphology and nanoscale properties of tribofilms. tribology international. 2011;44(3):201-10.
66. M.A. Nicholls PRN, G.M. Bancroft, M. Kasrai, T. Dob, B.H. Frazerc and G. De Stasio. Nanometer scale chemomechanical characterization of antiwear films. Tribology Letters. 2004;17(2):205-16.
67. Crobu M, Rossi A, Mangolini F, Spencer ND. Tribochemistry of bulk zinc metaphosphate glasses. Tribology letters. 2010;39(2):121-34.
68. Spikes H. The history and mechanisms of ZDDP. Tribology Letters. 2004;17(3):469-89.
69. Yin Z, Kasrai M, Fuller M, Bancroft GM, Fyfe K, Tan KH. Application of soft X-ray absorption spectroscopy in chemical characterization of antiwear films generated by ZDDP Part I: the effects of physical parameters. Wear. 1997;202(2):172-91.
70. Martin JM, Grossiord C, Le Mogne T, Bec S, Tonck A. The two-layer structure of Zndtp tribofilms: Part I: AES, XPS and XANES analyses. Tribology international. 2001;34(8):523-30.
71. S. Bec AT, J. M. Georges, R. C. Coy, J. C. Bell and G. W. Roper. Relationship between mechanical properties and structures of zinc dithiophosphate anti-wear films. Proceedings of the Royal Society A: Mathematical, Physical and Engineering Science. 1999;445(1992):4181-203.
72. Demmou K, Bec S, Loubet J-L, Martin J-M. Temperature effects on mechanical properties of zinc dithiophosphate tribofilms. Tribology international. 2006;39(12):1558-63.
73. Rossi A, Piras F, Kim D, Gellman A, Spencer N. Surface reactivity of tributyl thiophosphate: effects of temperature and mechanical stress. Tribology Letters. 2006;23(3):197-208.
74. De Donato P, Mustin C, Benoit R, Erre R. Spatial distribution of iron and sulphur species on the surface of pyrite. Applied Surface Science. 1993;68(1):81-93.
75. Zerulla D, Mayer D, Hallmeier K, Chassé T. Angular-resolved XANES measurements of the polar and azimuthal orientation of alkanethiols on InP (110). Chemical physics letters. 1999;311(1):8-12.

76. Heuberger RC. Combinatorial study of the tribochemistry of anti-wear lubricant additives: Diss., Eidgenössische Technische Hochschule ETH Zürich, Nr. 17207, 2007; 2007.
77. Brow RK, Tallant DR, Myers ST, Phifer CC. The short-range structure of zinc polyphosphate glass. Journal of Non-Crystalline Solids. 1995;191(1):45-55.
78. Nicholls MA, Do T, Norton PR, Kasrai M, Bancroft GM. Review of the lubrication of metallic surfaces by zinc dialkyl-dithiophosphates. Tribology international. 2005;38(1):15-39.
79. Wang W, Wong P, Zhang Z. Experimental study of the real time change in surface roughness during running-in for PEHL contacts. Wear. 2000;244(1):140-6.
80. Jamari J. Running-in of rolling contacts: University of Twente; 2006.